2022 IEEE Vehicle Power and Propulsion Conference (VPPC) | 978-1-6654-7587-7/22/$31.00 ©2022 IEEE | DOI: 10.1109/VPPC55846.2022.10003396

A Multi-Agent Approach to Landing Speed Control with Angular Rate Stabilization for Multirotors

[1]Binh-Minh Nguyen, [2]Shinji Hara, [3]Vu Phi Tran
[1]The University of Tokyo, [2]Tokyo Institute of Technology, [3]University of New South Wales
Email address of the corresponding author: [1]nguyen.binhminh@edu.k.u-tokyo.ac.jp

***Abstract* - To properly design the motion controller for multirotor, it is essential to address the propeller dynamics and their physical interaction. However, the complexity of system design increases together with the number of propellers. Considering this issue, this paper investigates the landing speed control system of the quadrotor as a case of study. The system consists of a vertical speed controller, and three roll-rate, pitch-rate, and yaw-rate controllers. We show that the system can be effectively modelled based on the concept of generalized frequency variable. This model allows the system stability to be analyzed via a simple inequality test or a graphical test, thereby, alleviating the design burden. The effectiveness of the proposed approach is demonstrated using a real quadrotor model.**

Keywords* - *generalized frequency variable, motion control, multi-agent system, propeller, quadrotor, stability analysis.

I. INTRODUCTION

Multirotor has been expected to be widely utilized due to its unique qualities, such as vertical takeoff and landing, hovering, and structural simplicity [1]. Consequently, motion control of multirotor has seen great growth since the last decade. Various methods have been proposed to improve the position and attitude tracking under the influences of model uncertainty, load variation, disturbance from the environment, and the faults of sensors and/or actuators [2] – [12].

Unfortunately, the previous works [1] – [12] treated the multirotor as a point mass moving in three-dimensional Euclidean space. However, the global motion of the multirotor is generated by the physical interaction between the propellers. Transparently, the multirotor should be treated as a multi-agent-system (MAS), in which each local agent is a propeller actuator. By both theoretical analysis and experiments, [13] recently showed that the local propellers and their interaction must be addressed properly to stabilize the overall multirotor system. Certainly, the complexity level of system design increases together with the number of the actuators. To deal with this issue, [13] showed that the absolute-stability of the altitude control system can be analyzed via a feedback connection of a transfer function and the sector-bounded nonlinear thrust model. In [13], the absolute stability is verified graphically using the Circle Popov criterion [14]. However, this approach is inconvenient for an integrated motion control system, which also considers the roll, pitch, and yaw motion controllers. The reason is due to the fact that the Circle Popov criterion of the integrated motion control system is graphically unavailable. Thus, the following question is still an open challenge: For the sake of practical application, how should we model and analyze the integrated motion control system of multirotor?

This paper considers the quadrotor, which is the most basic multirotor prototype. To guarantee the safe and stable landing motion, this paper investigates an integrated control system consisting of a vertical speed controller, and three roll-, pitch-, and yaw-rate controllers. Although the system is quite complex, it can be modelled as an MAS with the concept of generalized frequency variable (GFV) [15]. Consequently, the system stability is discussable from: (i) the GFV transfer function; (ii) the set of eigenvalues of the MAS's interconnection matrix. This approach is systematical, and can be extended to the other multirotor prototypes. Moreover, this model allows us an inequality test and a graphical test of system stabilization. The tests are very simple, thereby, alleviating the design burden.

The rest of this paper is organized as follows. Section II describes the landing control system with respect to the existence of the actuators. Section III presents the problem setting and the GFV approach. The effectiveness of the proposal is demonstrated using a real quadrotor in Section IV. Finally, the conclusions and future works are stated in Section V.

II. MODELING

This paper examines the quadrotor model with the rotor ordering shown in Fig. 1. F_i is the thrust, and ω_i is the rotational speed of the propeller number i. F_z is the total thrust acting at the center of gravity. The total mass of the quadrotor is m, and g is the acceleration of gravity. Let ϕ, θ, and γ be the roll, pitch, and yaw angle of the quadrotor; and let $J_{x(y,z)}$ be the quadrotor's moment of inertia along x (y, z) axis of the body-fixed frame. The roll and pitch moment arms are denoted and L_ϕ and L_θ, respectively. The relationship between F_i and ω_i is characterized by a nonlinear map Ψ, as shown in Fig. 2. This map is commonly approximated as a polynomial based on experimental data. The landing control system is generally expressed as in Fig. 3 with a hierarchical configuration.

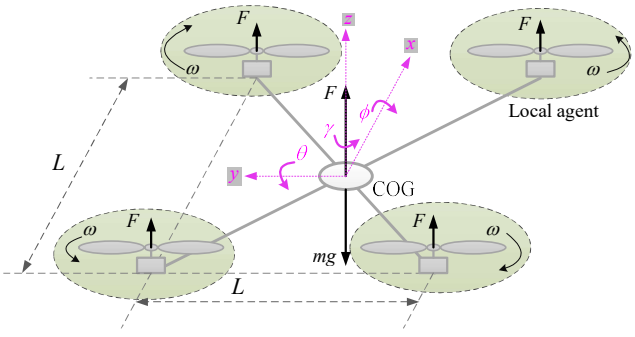

Fig. 1. Quadrotor model with rotor ordering.

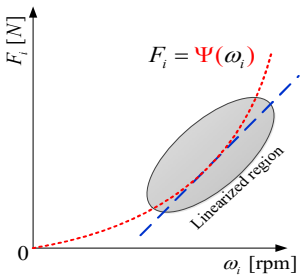

Fig. 2. Thrust characteristic.

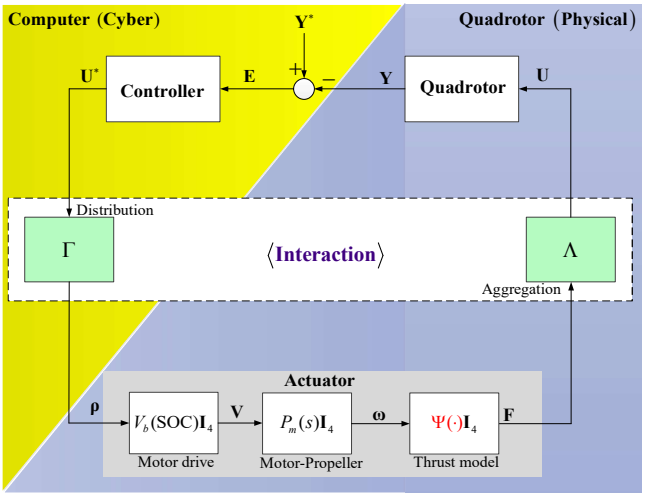

Fig. 3. Block diagram of the quadrotor's landing control system.

A. Lower-layer: Local actuator dynamics

Let ρ_i be the pulse width modulation (PWM) command and V_i be the voltage applied to motor i. We have $V_i = \rho_i V_b$. The voltage V_b of the battery is an decreasing function of the state of charge (SOC). The transfer function from V_i to ω_i is

$$P_m(s) = \frac{K_m}{T_m s + 1} \quad \cdots\cdots (1)$$

where the gain K_m and the time constant T_m are derived from the motor-propeller parameters. $\mathbf{I}_4$ is the identity matrix of size 4, which is used to express the multi-actuator dynamics in the lower-layer. Besides, the column vectors $\boldsymbol{\rho}$, $\mathbf{V}$, $\boldsymbol{\omega}$ and $\mathbf{F}$ include ρ_i, V_i, ω_i and F_i, respectively.

B. Middle-layer: Interaction

In Fig. 3, the force-torque vector $\mathbf{U}$ is defined as

$$\mathbf{U} = \begin{bmatrix} F_z & \tau_\phi & \tau_\theta & \tau_\gamma \end{bmatrix}^{\mathrm{T}} \quad \cdots\cdots (2)$$

where τ_ϕ, τ_θ, and τ_γ are the roll-, pitch-, and yaw-moment acting on the center of gravity (COG) of the quadrotor. $\mathbf{U}$ is aggregated from $\mathbf{F}$ via the aggregation matrix

$$\Lambda = \begin{bmatrix} 1 & 1 & 1 & 1 \\ -\frac{L_\phi}{2} & -\frac{L_\phi}{2} & \frac{L_\phi}{2} & \frac{L_\phi}{2} \\ \frac{L_\theta}{2} & -\frac{L_\theta}{2} & \frac{L_\theta}{2} & -\frac{L_\theta}{2} \\ K_\gamma & -K_\gamma & -K_\gamma & K_\gamma \end{bmatrix} \quad \cdots\cdots (3)$$

where K_γ is the yaw moment constant. The command vector $\mathbf{U}^*$ is distributed to $\boldsymbol{\rho}$ via the distribution matrix

$$\Gamma = \frac{1}{K_f}\begin{bmatrix} \frac{1}{4} & -\frac{1}{2L_\phi} & \frac{1}{2L_\theta} & \frac{1}{4K_\gamma} \\ \frac{1}{4} & -\frac{1}{2L_\phi} & -\frac{1}{2L_\theta} & -\frac{1}{4K_\gamma} \\ \frac{1}{4} & \frac{1}{2L_\phi} & \frac{1}{2L_\theta} & -\frac{1}{4K_\gamma} \\ \frac{1}{4} & \frac{1}{2L_\phi} & -\frac{1}{2L_\theta} & \frac{1}{4K_\gamma} \end{bmatrix} \quad \cdots\cdots (4)$$

where K_f is the linearized gain from the PWM command to the thrust force.

C. Upper-layer: Global quadrotor dynamics

For the safe and stable landing purpose, the output vector and its reference vector can be selected as

$$\mathbf{Y} = \begin{bmatrix} v_z & v_\phi & v_\theta & v_\gamma \end{bmatrix}^{\mathrm{T}}, \ \mathbf{Y}^* = \begin{bmatrix} v_z^* & v_\phi^* & v_\theta^* & v_\gamma^* \end{bmatrix}^{\mathrm{T}} \quad \cdots\cdots (5)$$

From [1], the global dynamics of the quadrotor is given as

$$\begin{cases} \dot{z} = v_z, \ \dot{v}_z = (\cos\phi\cos\theta)\dfrac{F_z}{m} - g - d_z \\ \dot{\phi} = v_\phi, \ \dot{v}_\phi = \dfrac{J_y - J_z}{J_x}\dot{\theta}\dot{\gamma} + \dfrac{\tau_\phi}{J_x} - d_\phi \\ \dot{\theta} = v_\theta, \ \dot{v}_\theta = \dfrac{J_z - J_x}{J_y}\dot{\gamma}\dot{\phi} + \dfrac{\tau_\theta}{J_y} - d_\theta \\ \dot{\gamma} = v_\gamma, \ \dot{v}_\gamma = \dfrac{J_x - J_y}{J_z}\dot{\phi}\dot{\theta} + \dfrac{\tau_\gamma}{J_z} - d_\gamma \end{cases} \quad \cdots\cdots (6)$$

where $d_{z,\phi,\theta,\gamma}$ are the external disturbances to the quadrotor. The tracking error vector $\mathbf{E} = \mathbf{Y}^* - \mathbf{Y}$ is the input of the controller which generates the command vector $\mathbf{U}^*$.

III. GFV APPROACH

A. Problem setting

As presented in [13] and [16], the control system of the quadrotor might include the disturbance observer for improving the robustness, the state observer for estimating the unknown variables, and the Kalman filter for compensating the sensor delay. The aforementioned controllers are not considered in this paper. This paper provides a different approach by only focusing on landing speed control. To this end, we apply GFV method based on a linearized model around an equilibrium speed of the propeller, and investigate the stability. We make the following assumptions.

Assumption 1: The quadrotor is assumed to be close to the vertical motion, so that $F_z \approx mg$. It is also assumed that the roll and pitch motions are slight that $\sin\phi \approx \phi$ and $\sin\theta \approx \theta$.

Assumption 2: Good measurements of the quadrotor speed and roll-, pitch-, yaw-rate are available.

We can omit the position variables and the Euler angles in (6), since we only consider the controls of vertical speed and Euler angles' rates in this paper. Then, under Assumption 1, the dynamical model (6) can be linearized as follows

$$\begin{cases} \dot{v}_z = \dfrac{F_z}{m} - g - d_z \\ \dot{v}_\phi = \dfrac{\tau_\phi}{J_x} - d_\phi \\ \dot{v}_\theta = \dfrac{\tau_\theta}{J_y} - d_\theta \\ \dot{v}_\gamma = \dfrac{\tau_\gamma}{J_z} - d_\gamma \end{cases} \quad \cdots\cdots (7)$$

It can be derived from Assumption 1 that the quadrotor always operates in a certain region of the thrust characteristics in Fig. 2. Focusing on this region, the relationship between the thrust force and the propeller speed can be linearized as

$$F_i = \kappa \omega_i \quad \cdots\cdots (8)$$

Notice 1: The above linearization is reasonable as seen in Fig. 7, which shows the thrust characteristic obtained from the experimental results of our quadrotor system.

As mentioned above, this paper considers the controller as

$$diag\left\{C_z(s), C_\phi(s), C_\theta(s), C_\gamma(s)\right\} \quad \cdots\cdots (9)$$

where $C_z(s)$ is the vertical speed controller, and $C_{\phi,\theta,\gamma}$ are the roll-, pitch-, yaw-rate controllers. The dynamics of the vertical speed, roll-rate, pitch-rate, and yaw-rate has a common term of $1/s$. Hence, the four controllers in (9) can be selected as

$$C_\#(s) = \alpha_\# C_o(s), \ \# \in \{z, \ \phi, \ \theta, \ \gamma\} \quad \cdots\cdots (10)$$

where $C_o(s)$ is the common controller, and $\alpha_\#$ is a positive gain to be selected for each control channel. In summary, the block diagram of the upper-layer can be described as in Fig. 4 where

$$\xi = \left[m(g + d_z) \ \ J_x d_\phi \ \ J_y d_\theta \ \ J_z d_\gamma\right]^{\mathrm{T}} \quad \cdots\cdots (11)$$

B. Stability analysis

The landing control system is equivalently expressed as an MAS in Fig. 5, where each local agent is an actuator sub system. The equivalent vector and matrices are defined as

$$\tilde{\xi} = \left[g + d_z \ \ d_\phi \ \ d_\theta \ \ d_\gamma\right]^{\mathrm{T}} \quad \cdots\cdots (12)$$

$$\tilde{\Lambda} = diag\left\{\frac{1}{m}, \frac{1}{J_x}, \frac{1}{J_y}, \frac{1}{J_z}\right\}\Lambda \quad \cdots\cdots (13)$$

$$\tilde{\Gamma} = \Gamma diag\left\{\alpha_z, \alpha_\phi, \alpha_\theta, \alpha_\gamma\right\} \quad \cdots\cdots (14)$$

Reorganizing Fig. 5, the system stability can be analyzed from the interconnection system in Fig. 6 where

$$H(s) = \frac{V_b \kappa}{s} C_o(s) P_m(s) \quad \cdots\cdots (15)$$

$$Q = -\tilde{\Lambda}\tilde{\Gamma} \quad \cdots\cdots (16)$$

where Q represents the interaction between the local agent. The total system stability can be analyzed from the transfer function

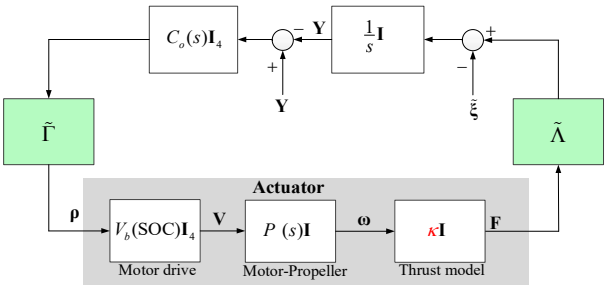

Fig. 5. Linearized block diagram of the landing control system.

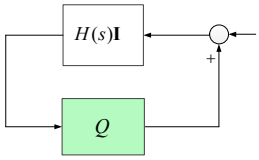

Fig. 6. Representation of landing speed control system as a MAS.

$$G(s) = \left[\frac{1}{H(s)}\mathbf{I}_4 - Q\right]^{-1} \quad \cdots\cdots (17)$$

Now, define the transfer function

$$L(s) = \left[s\mathbf{I}_4 - Q\right]^{-1} \quad \cdots\cdots (18)$$

Replacing "s" in $L(s)$ with $\Phi(s) := 1/H(s)$, we will have $G(s) = L(\Phi(s))$. Therefore, we can say that the system shown in Fig. 6 has the generalized frequency variable (GFV) $\Phi(s)$. We define the complex plane and the closed right-half plane as $\mathcal{C}$ and $\mathcal{C}_+$, respectively. Hence, we can analyze system stability by defining the following domains

$$\Omega_+ := \Phi(\mathcal{C}_+), \ \Omega_+^c = \mathcal{C} \setminus \Omega_+ \quad \cdots\cdots (19)$$

Applying Theorem 1 in [15], we have

General stability condition: Under the Assumptions 1 and 2 and the problem setting presented in the previous sub-section, the landing control system is said to be stable if we can design $C_o(s)$ and a set of positive scalars $\alpha_{\neq}(\neq \in \{z, \phi, \theta, \gamma\})$ such that all the eigenvalues of matrix Q are located in Ω_+^c.

From (13), (14) and (16), it can be derived that

$$Q = -diag\left\{\frac{\alpha_z}{mK_f}, \frac{\alpha_\phi}{J_x K_f}, \frac{\alpha_\theta}{J_y K_f}, \frac{\alpha_\gamma}{J_z K_f}\right\} \quad \cdots\cdots (20)$$

Hence, the eigenvalues λ_i $(i \in \{1, 2, 3, 4\})$ of matrix Q are given by the diagonal elements shown in (20).

C. Stability test: PI controller case

It should be emphasized that the advantage of the GFV approach is that the order of the system for the stability check is that of $H(s)$, which is four times smaller than that of the whole system. This makes the stability test very simpler. To demonstrate this, we here consider the case of proportional-

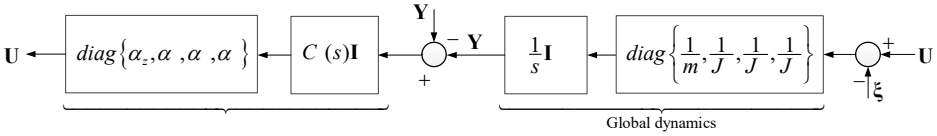

Fig. 4. Block diagram of the upper-layer.

integral (PI) type controller. Without loss of generality, the common controller $C_o(s)$ can be expressed as:

$$C_o(s) = \frac{s+\sigma}{s} \quad \cdots\cdots (21)$$

Substituting (21) into (15), the GFV can be derived as

$$\Phi(s) = \frac{1}{H(s)} = \frac{s^3 + cs^2 + ds + e}{as + b} = \frac{l(s)}{n(s)} \quad \cdots\cdots (22)$$

where

$$a = \frac{V_b \kappa K_m}{T_m}, b = \frac{V_b \kappa K_m \sigma}{T_m}, c = \frac{1}{T_m}, d = e = 0 \quad \cdots\cdots (23)$$

Let $\lambda = x + jy$ where j is the imaginary unit, we define

$$\begin{aligned} pl(\lambda, s) &= l(s) - \lambda n(s) \\ &= s^3 + (p_1 + jq_1)s^2 + (p_2 + jq_2)s + (p_3 + jq_3) \end{aligned} \quad (24)$$

where

$$\begin{cases} p_1 = c,\ q_1 = 0 \\ p_2 = d - ax,\ q_2 = -ay \\ p_3 = e - bx,\ q_3 = -by \end{cases} \quad \cdots\cdots (25)$$

Following Theorem 1 in [15], the stable region Ω_+^c is defined by a set of inequalities $\{D_i(x,y) > 0, i = 1,2,3\}$ where

$$D_1 = p_1,\ D_2 = \det\begin{vmatrix} p_1 & p_3 & -q_2 \\ 1 & p_2 & -q_1 \\ 0 & q_2 & p_1 \end{vmatrix},\ D_3 = \det\begin{vmatrix} p_1 & p_3 & 0 & -q_2 & 0 \\ 1 & p_2 & 0 & -q_1 & -q_3 \\ 0 & p_1 & p_3 & 0 & -q_2 \\ 0 & q_2 & 0 & p_1 & p_3 \\ 0 & q_1 & q_3 & 1 & p_2 \end{vmatrix}$$

Remark 1: Q is a diagonal matrix with real negative eigenvalues λ_i. Hence, the stability condition can be checked via the stability of four feedback connections of $H(s)$ and λ_i. With respect to the GFV (22), the control system is stable if the following third-order polynomial has all roots in the open left half plane for all i from 1 to 4: $pl(s) = s^3 + cs^2 - \lambda_i as - \lambda_i b$. Following the Routh-Hurwitz criterion, it is required that

$$\begin{cases} c > 0,\ -\lambda_i a > 0,\ -\lambda_i b > 0\ \forall i \in \{1,2,3,4\} \\ c(-\lambda_i a) > (-\lambda_i b) \end{cases} \quad \cdots\cdots (26)$$

From (23) and (26), the stability condition of the overall system is finally obtained as

$$\sigma < \frac{1}{T_m} \quad \cdots\cdots (27)$$

IV. Demonstration

A. Quadrotor model

To demonstrate the above approach, this study utilizes the quadrotor which has been used recently in [13] and [16]. The main parameters of the quadrotor are summarized in TABLE I, and the nonlinear thrust model is shown in Fig. 7. Considering the operating points about the propeller speed of 12,000 [rpm], the linearized gain in (8) can be approximately calculated as $\kappa \approx 2.83 \times 10^{-4} [N/rpm]$.

B. Test results and discussion

Let the transfer function of the common plant be

TABLE I. Physical parameters of the quadrotor

Total mass	$m = 1.12$ [kg]
Roll moment of inertia	$J_x = 1.0 \times 10^{-2} [kgm^2]$
Pitch moment of inertia	$J_y = 8.2 \times 10^{-3} [kgm^2]$
Yaw moment of inertia	$J_z = 1.48 \times 10^{-2} [kgm^2]$
Pitch & roll moment arms	$L_\phi = 0.21$[m], $L_\theta = 0.18[m]$
Yaw moment constant	$K_\gamma = 0.0492[Nm]$
Battery voltage (fully charged)	$V_b = 11.7[V]$
Motor's amplifying gain	$K_m = 2100[rpm/V]$
Motor's time constant	$T_m = 0.004[s]$

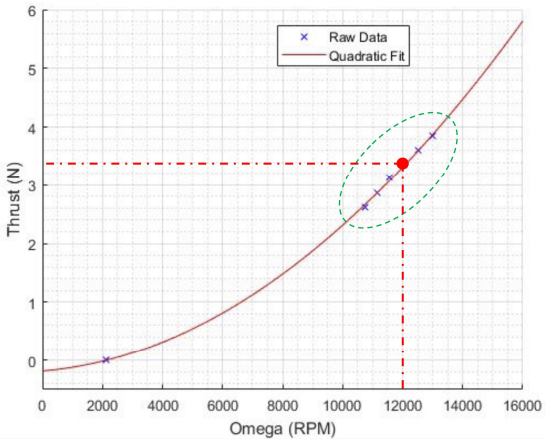

Fig. 7. Thrust characteristic of the quadrotor under study.

$$P_o(s) = \frac{1}{s} \quad \cdots\cdots (28)$$

Considering the quadrotor body dynamics (7), the transfer function of the vertical speed, roll-rate, pitch-rate, and yaw-rate are expressed as

$$P_z(s) = \frac{P_o(s)}{m}, P_\phi(s) = \frac{P_o(s)}{J_x}, P_\theta(s) = \frac{P_o(s)}{J_y}, P_\gamma(s) = \frac{P_o(s)}{J_z} \quad (29)$$

It should be emphasized that the derived stability condition (27) is essential to decide the ratio of PI gains to guarantee the stability of the multirotor. (27) requires the ratio σ to be bounded by $1/T_m$. This means that the neglect of the actuator dynamics, i.e., assuming $T_m = 0$, as done in the traditional approach may cause a trouble of losing the stability. In other words, designed controller by neglecting the actuator dynamics which stabilizes $P_o(s)$ may not stabilize $P_o(s)P_m(s)$ if σ is really large. We now consider the following test confirm this.

The quadrotor is landing from the altitude of 2 [m]. The reference landing speed is set to -0.1 $[m/s]$, and the roll-rate, pitch-rate, yaw-rate are required to be maintained at 0 $[rad/s]$. Two cases were conducted as follows.

Case A: The integral gain of the common controller is selected as $\sigma = 338.5$. The scale parameters are selected as $\{\alpha_{z,\phi,\theta,\gamma}\} = \{10m, 14J_x, 13J_y, 15J_z\}$. With this selection of the controller, matrix Q has four real eigenvalues of $\{-1.96, -2.34, -2.54, -2.94\}$. It is easily to verify that the closed loop system $\{C_o(s), P_o(s)\}$ is stable with this selection. Unfortunately, the overall system is unstable since the inequality (27) is not satisfied

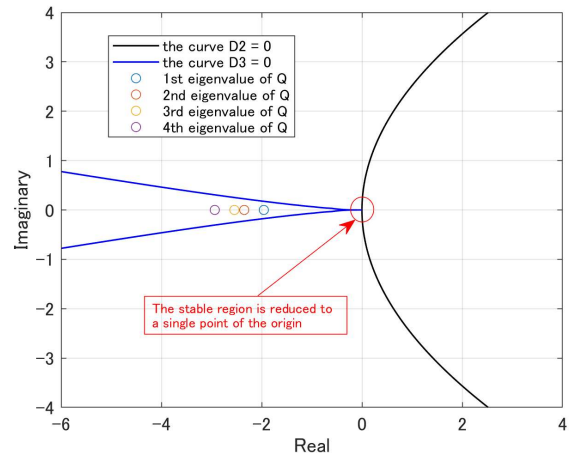

(a) Graphical test

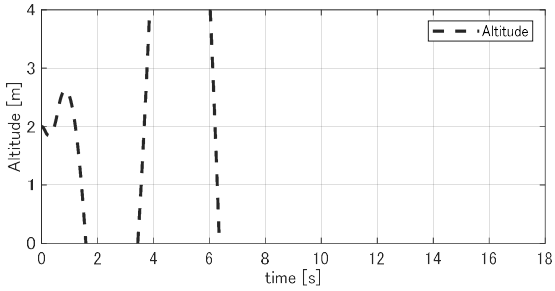

(b) Altitude

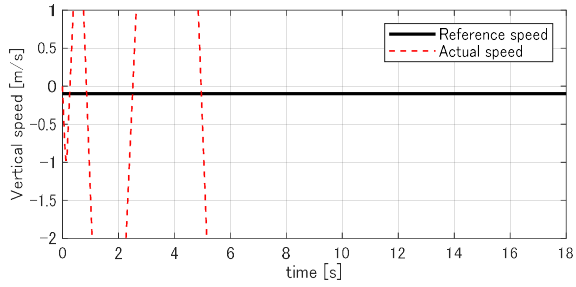

(c) Vertical speed

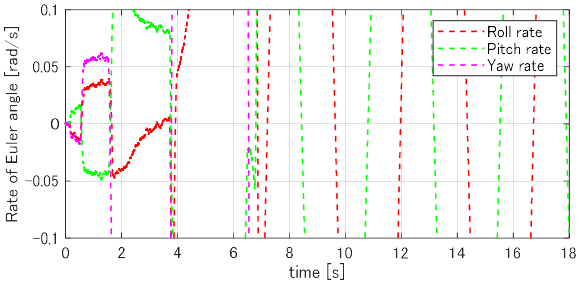

(d) Rates of Euler angles

Fig. 8. Case A (unstable example).

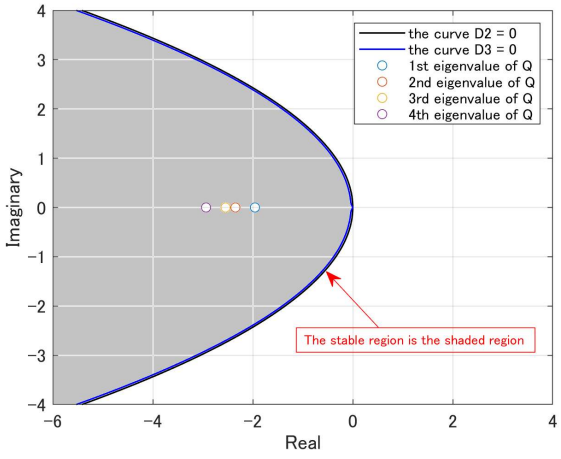

(a) Graphical test

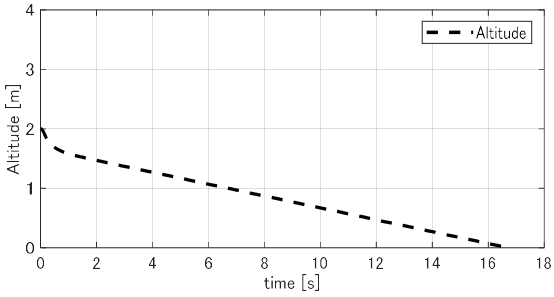

(b) Altitude

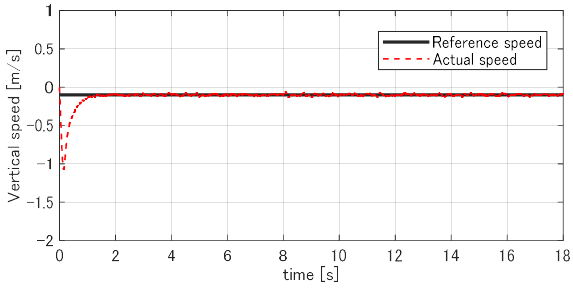

(c) Vertical speed

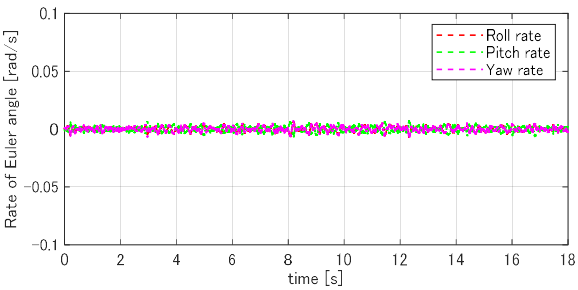

(d) Rates of Euler angles

Fig. 9. Case B (stable example).

$$338.5 = \sigma > \frac{1}{T_m} = 250.0 \quad \cdots\cdots (29)$$

The stable region in this test is reduced to a single point (the origin), as shown in Fig. 8(a). In other words, all the eigenvalues of matrix Q are not located in the stable region. As can be seen from Fig. 8(b), the altitude of the quadrotor experiences a large fluctuation, which means the quadrotor hits the ground seriously. As shown in Fig. 8(c), the vertical speed is unstable and cannot follow the reference values. Also, Fig. 8(d) shows that the rates of all Euler angles (roll-rate, pitch-rate, and yaw-rate) reach really large values. In summary, the quadrotor really suffers an accident, and it cannot land safely.

Case B: The integral gain of the common controller is selected as $\sigma = 3.33$. Similarly to the previous test, the scale parameters are selected as $\{\alpha_{z,\phi,\theta,\gamma}\} = \{10m, 12J_x, 13J_y, 15J_z\}$. These parameters are selected via a tuning process such that the control performance is fairly acceptable. Now, it can be verified that the inequality (27) is satisfied

$$3.33 = \sigma < \frac{1}{T_m} = 250.0 \quad \cdots\cdots (30)$$

As shown in Fig. 9(a), all the eigenvalues of matrix Q are located in the stable region. We can conclude that the quadrotor control system is stable in this test case. As shown in Fig. 9(b), the altitude of the quadrotor is gradually reduced to zero. The vertical speed can quickly match with the reference values, as can be seen from Fig. 9(c). Also, Fig. 9(d) shows that all the roll-rate, pitch-rate, and yaw-rate are maintained around zero. Although the desired speed is $-0.1\ [m/s]$, the landing time is about 16 seconds, due to a peak of the quadrotor's speed at the beginning. To improve the speed tracking performance, a robust controller, such as PI controller with disturbance observer can be considered in future.

In summary, the inequality test (27) and the graphical test give the same conclusion on system stability. The test conveys a *glocal meaning* in the following sense. The parameter T_m belongs to the local actuator. On the other hand, σ belongs to the setting of the global motion controllers, which should be limited by the capacity of the local actuator. For install, small T_m means the motor drive is fast and has enough bandwidth. Consequently, we will have more freedom to select the global controller.

Remark 2: Actually, the uncertainties exist due to several reasons. For instance, the model parameters in the distribution matrix Γ are not necessarily similar to the physical parameters of the aggregation matrix Λ. On the other hand, the variation of the operating point in Fig. 7 is worth examined. Fortunately, matrix Q can be shown to be diagonal. Hence, we might utilize a recent result on robust stability analysis [17] without special difficulty. Together with the inequality (27), such analysis will give additional constraints of the control parameters.

Remark 3: If the quadrotor speed is not measurable, it can be estimated using on-board sensors. If the sensor delays exist, they can be compensated using Kalman filter [16] or [18].

V. CONCLUSIONS

This paper explains why the multirotor motion control system must be treated as a multi-agent system with physical interaction for properly guaranteeing system stability. As a case of study, this paper shows that the landing control system of the quadrotor can be effectively modelled with generalized frequency variable. This modelling allows us to check system stability via a simple inequality test or a graphical test. It is interesting that the tests' complexity levels does not rely on the number of propellers. By demonstration using a real quadrotor model, the proposed approach is shown to be a promising tool for practical application. In the future steps, we will evaluate the proposed approach by both numerical simulation and experimental tests. We will also utilize the proposed approach to design advanced algorithms, such as disturbance observer and fault tolerance control with robust stability analysis.

ACKNOWLEDGEMENT

This work is partly supported by the JSPS Grants-in-Aid for Scientific Research No. 22K14283 and the Nagamori Research Grant 2022.

REFERENCES

[1] R. Rashad, J. Goerres, R. Aarts, J. B. C. Engelen and S. Stramigioli, "Fully Actuated Multirotor UAVs: A Literature Review," in IEEE Robotics & Automation Magazine, Vol. 27, No. 3, pp. 97-107, 2020.

[2] P. E. I. Pounds, D. R. Bersak, and A. M. Dollar, "Stability of Small-Scale UAV Helicopter and Quadrotors with Added Payload Mass Under PID Control," Autonomous Robots, Vol. 33, pp. 129-142, 2012.

[3] R. Perez-Alcocer, J. Moreno-Valenzuela, and R. Miranda-Colorado, "ARobust Approach for Trajectory Tracking Control of a Quadrotor with Experimental Validation," ISA Transactions, Vol. 65, pp. 262–274, 2016.

[4] X. Lyu, J. Zhou, H. Gu, Z. Li, S. Shen, and F. Zhang, "Disturbance Observer Based Hovering Control of Quadrotor Tail-Sitter VTOL UAVs Using H_∞ Synthesis," IEEE Robotics and Automtion Letters, Vol. 3, No. 4, pp. 2910-2917, 2018.

[5] X-M. Nguyen and S-K. Hong, "Improved Altitude Control Algorithm forQuadcop ter Unmanned Aerial Vehicles," Applied Sciences 9, No. 10: 2122, 2019.

[6] M. Sharma and I. Kar, "Nonlinear Disturbance Observer Based GeometricControl of Quadrotors," Asian Journal of Control, Vol. 23, Iss. 4, pp. 1936-1951, 2021.

[7] A. Al-Mahturi, F. Santoso, M. A. Garratt and S. G. Anavatti, "Self-Learningin Aerial Robotics Using Type-2 Fuzzy Systems: Case Study in Hovering Quadcopter Flight Control," IEEE Access, Vol. 9, pp. 119520-119532, 2021.

[8] A. Merheb, H. Noura and F. Bateman, "Passive Fault Tolerant Control of Quadrotor UAV Using Regular and Cascaded Sliding Mode Control," 2013 Conference on Control and Fault-Tolerant Systems, pp. 330-335, 2013.

[9] Y. Zhong, Y. Zhang, W. Zhang, J. Zuo and H. Zhan, "Robust Actuator Fault Detection and Diagnosis for a Quadrotor UAV With External Disturbances," IEEE Access, Vol. 6, pp. 48169-48180, 2018.

[10] W. Chung and H . Son, "Fault-Tolerant Control of Multirotor UAVs by Control Variable Elimination," IEEE/ASME Transactions on Mechatronics, Vol. 25, No. 5, pp. 2513-2522, 2020.

[11] S. Sun, X. Wang, Q. Chu and C. D. Visser, "Incremental Nonlinear Fault-Tolerant Control of a Quadrotor With Complete Loss of Two Opposing Rotors," in IEEE Transactions on Robotics, Vol. 37, No. 1, pp. 116-130, 2021.

[12] M. A. Ashraf, S. Ijaz, U. Javaid, S. Hussain, H. Anwaar and M. Marey, "A Robust Sensor and Actuator Fault Tolerant Control Scheme for Nonlinear System," IEEE Access, Vol. 10, pp. 626-637, 2022.

[13] B-M. Nguyen, T. Kobayashi, K. Sekitani, M. Michihiro, and T. Narikiyo, "Altitude Control of Quadcopter Flying Vehicles with Absolute Stability Analysis," IEEJ Transactions on Industry Applications, Vol. 11, No. 4, 2022.

[14] H. K. Khalil, "Nonlinear Systems," Prentice Hall, 2002.

[15] S. Hara, H. Tanaka and T. Iwasaki, "Stability Analysis of Systems With Generalized Frequency Variables," in IEEE Transactions on Automatic Control, Vol. 59, No. 2, pp. 313-326, 2014.

[16] K. Yoshimura, B-M. Nguyen, H. Fujimoto, M. Kawanishi, and T. Narikiyo, "Dual-Rate Altitude Control of Drones Based on Double-Layer Kalman Filter," 8th IEEJ International Workshop on Sensing, Actuation, Motion Control, and Optimization, pp. 485-488, 2022.

[17] S. Hara, T. Iwasaki, and Y. Hori, "Robust Stability Analysis for LTI Systems with Generalized Frequency Variables and Its Application to Gene Regulatory Networks," Automatica, Vol. 105, pp. 96-106, 2019.

[18] B-M. Nguyen, W. Ohnishi, Y. Wang, H. Fujimoto, Y. Hori, K. Ito, M. Odai, H. Ogawa, E. Takano, T. Inoue, and M. Koyama, "Dual Rate Kalman Filter Considering Delayed Measurement and Its Application in Visual Servo," 13th IEEE International Workshop on Advanced Motion Control (AMC), pp. 494-499, 2014 (doi: 10.1109/AMC.2014.6823331).